

Stability of Unduloidal and Nodoidal Menisci between two Solid Spheres

Boris Y. Rubinstein and Leonid G. Fel

Mathematics Subject Classification (2010). Primary 53A10; Secondary 76B45.

Keywords. Stability problem, Axisymmetric pendular rings, Inflection points.

Abstract. We find the existence conditions of unduloidal and nodoidal menisci between two solid spheres and study their stability in the framework of non-spectral theory of stability of axisymmetric menisci between two axisymmetric solid bodies in the absence of gravity.

1. Introduction

Pendular rings (PR) in the absence of gravity between two axisymmetric solid bodies (SB) with free contact lines (CL) are surfaces of revolution with constant mean curvature (CMC) classified by Delaunay in [1]: cylinder (Cyl), sphere (Sph), catenoid (Cat), nodoid (Nod) and unduloid (Und). Two questions are important in this regard: what is an exact shape (meniscus) of PR in the given setup and how stable is it. The first question would be answered once one could find a solution of the Young-Laplace equation (YLE) supplemented with boundary conditions (BC) of free CL and given PR volume. Recent progress [7] in the PR problem has shown an existence of multiple solutions of YLE for given PR volume and as a consequence poses a question on menisci stability as a menisci selection rule.

There are two different approaches to study stability of PR between two SB with free CL. The first approach was initiated by T. Vogel [9, 10] and based on the study of the Sturm-Liouville equation (SLE) and its spectrum. Implementation of this approach is a difficult task: only several exact results for Cat [16], Sph [8] and Und (with special contact angle values) [3, 10] between two plates are known. Investigation of menisci between other surfaces encounters even more difficulties of finding analytically a spectrum of SLE with given shape of SB (Cyl [11] and convex Und and Nod between equal spheres [12, 14]).

Another approach was suggested recently [2] as a part of a variational problem with minimized and constrained functionals and free endpoints moving along two given planar curves S_1, S_2 . It is based on Weierstrass' formula of second variation

$\delta^2 W$ for isoperimetric problem. A freedom of endpoints allows to derive $\delta^2 W$ as a quadratic form in perturbations $\delta\phi_j$ of the endpoints ϕ_j along $S_j(\psi_j)$,

$$\delta^2 W = Q_{11} (\delta\psi_1)^2 + 2Q_{12} \delta\psi_1 \delta\psi_2 + Q_{22} (\delta\psi_2)^2, \quad Q_{ij} = Q_{ij}(\phi_2, \phi_1), \quad (1.1)$$

and find in the plane $\{\phi_1, \phi_2\}$ a stability domain Stab where $\delta^2 W \geq 0$ (see Theorem 4.1 in [2]). Stability of menisci between parallel plates were studied in [2] for all Delaunay's surfaces. We also have found Stab for Cat and Cyl between two SB: spheres, paraboloids, catenoids, ellipsoids and between sphere and plane. This approach has no limitations to find Stab analytically for arbitrary meniscus and SB shapes.

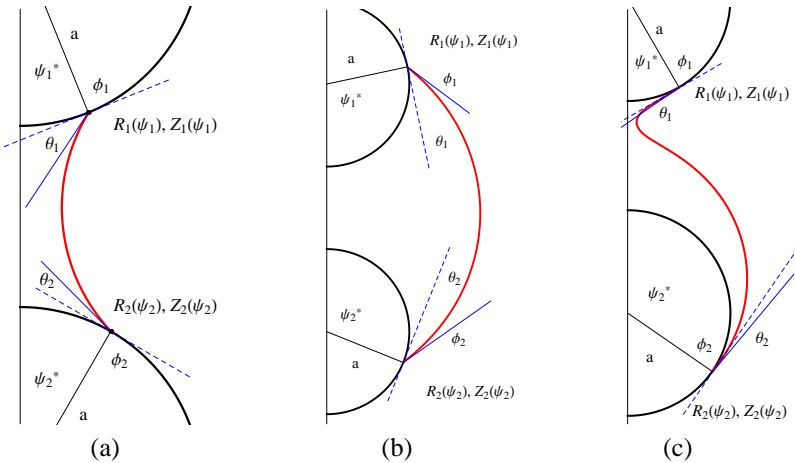


FIGURE 1. Sketches (meridional sections) of three menisci between two equal spheres of radius a showing the contact angles θ_1, θ_2 , filling angles ψ_1^*, ψ_2^* and coordinates of the endpoints ϕ_1, ϕ_2 : (a) concave meniscus, F-F setup, (b) convex meniscus, B-B setup, (c) meniscus with one inflection point, F-B setup.

The present paper deals with a more difficult case when **Und** and **Nod** menisci are trapped between equal solid spheres. Compared with menisci geometry between two plates, this problem leads to the question of *menisci existence* determined by **Und** and **Nod** geometry between two spheres. Thus, we have to consider the stability Stab and existence Exst domains such that $\text{Stab} \subseteq \text{Exst}$; to establish the latter we need a simple analytical geometry. We consider three different setups of semi-spheres (*face* and *back*) where the meniscus is approaches the spheres: *face-to-face* (F-F), *face-to-back* (F-B) and *back-to-back* (B-B).

The paper is organized in seven sections. In section 2 we consider four different types of constraints which define the existence of menisci between two convex SB (not necessarily spheres), and derive the conditions when they occur. In section 3 we specify them for the case of two solid spheres; we discuss their coexistence and establish Exst domain in different setups. In sections 4,5 and 6, based on Theorem 4.1 in [2], we give a detailed analysis of Stab domains for menisci between

equal spheres with F-F, B-B and F-B setups, respectively, and find the stable Und with two inflection points (IP). In section 7 we show how a non-equivalence of the spheres affects both Stab and Exst domains.

2. Axisymmetric menisci between solid bodies and their existence

Consider axisymmetric PR between two SB in absence of gravity. The axial symmetry of SB is assumed along z -axis (see Figure 1). The shapes of meniscus $\{r(\phi), z(\phi)\}$ and two SB $\{R_j(\psi_j), d_j + Z_j(\psi_j)\}$ are given in cylindrical coordinates. The filling angle ψ_j along the j -th solid-liquid interface satisfies $0 \leq \psi_j \leq \infty$ for unbounded SB and $0 \leq \psi_j < \infty$ for bounded SB.

Functions $r(\phi)$ and $z(\phi)$ are defined in the range $\phi_2 \leq \phi \leq \phi_1$ and satisfy YLE with curvature H ,

$$S_H = \frac{z'}{r(r'^2 + z'^2)^{1/2}} + \frac{z''r' - z'r''}{(r'^2 + z'^2)^{3/2}}, \quad (2.1)$$

where $S_H = \pm 1$ correspond to the menisci with positive and negative curvature H , respectively. Equation (2.1) is supplemented with Young (transversality) relations for given contact angles θ_j ,

$$\theta_j = (-1)^{j-1} \left(\arctan \frac{z'(\phi_j)}{r'(\phi_j)} - \arctan \frac{Z'(\psi_j^*)}{R'(\psi_j^*)} \right), \quad j = 1, 2, \quad \theta_j \geq 0, \quad (2.2)$$

and consistency equalities,

$$\begin{aligned} z(\phi_1) &= d_1 + Z_1(\psi_1^*), & r(\phi_1) &= R_1(\psi_1^*), \\ z(\phi_2) &= d_2 + Z_2(\psi_2^*), & r(\phi_2) &= R_2(\psi_2^*). \end{aligned} \quad (2.3)$$

where $d = d_1 - d_2$ is a distance between centers of S_1 and S_2 . Throughout this paper we make use of a standard parametrization [2] for menisci with $H \neq 0$ which goes back to [4, 5],

$$\begin{aligned} r(\phi) &= \sqrt{1 + B^2 + 2B \cos(S_H \phi)}, \\ z(\phi) &= M(S_H \phi, B) - M(S_H \phi_2, B) + Z_2(\psi_2^*), \\ M(\phi, B) &= (1 + B)E(\phi/2, m) + (1 - B)F(\phi/2, m), \quad m = 2\sqrt{B}/(1 + B). \end{aligned} \quad (2.4)$$

where $F(x, m)$ and $E(x, m)$ denote elliptic integrals of the first and the second kind. Formulas (2.4) describe four Delaunay's surfaces with nonzero curvature H : Cyl, $B = 0$; Und, $0 < B < 1$; Sph, $B = 1$ and Nod, $B > 1$. We assume that in the range $\phi_2 < \phi < \phi_1$ the ordinate $z(\phi)$ is a growing function $z(\phi_2) < z(\phi) < z(\phi_1)$. According to (2.4) we get

$$\Delta(\phi_1, \phi_2, S_H, B) = M(S_H \phi_1, B) - M(S_H \phi_2, B) > 0, \quad (2.5)$$

that determines S_H introduced in (2.1). This value cannot be defined when $z(\phi_1) = z(\phi_2)$ for $\phi_1 \neq \phi_2$. The condition (2.5) implies that all unduloids have positive curvature, i.e., $S_H = 1$. It follows from the explicit expression $z'(\phi) = S_H(1 + B \cos(S_H \phi))/r$, leading to positive $z'(\phi)$ for $B < 1$.

Once $r(\phi)$ and $z(\phi)$ are parameterized by (2.4) we have to determine the PR existence as a physically valid object. This leads to restriction on parameters B , ϕ_1 , ϕ_2 , important for nonplanar SB and makes the stability domain Stab substantially dependent on conditions of PR existence. This phenomenon was observed in [2] for Cat between two spheres and also announced in [14] for NOD between equal spheres with contact angles $90^\circ \leq \theta_j < 180^\circ$. In other words, a meniscus geometry has to satisfy requirements on B , ϕ_1 , ϕ_2 to avoid different types of meniscus nonexistence which can be distributed into four major types.

- **Type A:** *meniscus does not reach solid surface, Figure 2a*

This condition is applicable only to SB with finite maximal radial size R_{max} ,

$$1 + B^2 + 2B \cos \phi \geq R_{max}^2. \quad (2.6)$$

- **Type B:** *meniscus reaches solid surface with negative contact angle, Figures 2b and 3c.*

Let PR be trapped between two SB and let a contact angle θ_2 at S_2 be given. Consider S_1 and require $\theta_1 \geq 0$, otherwise the meniscus "pierces" S_1 and contacts it from "inside". The critical endpoint ϕ_1^s corresponding to $\theta_1 = 0$ satisfies three equalities:

$$\begin{aligned} z'(\phi_1^s)/r'(\phi_1^s) &= Z_1'(\psi_1^*)/R_1'(\psi_1^*), \quad r(\phi_1^s) = R_1(\psi_1^*), \\ z(\phi_1^s, \phi_2) &= d_1 + Z_1(\psi_1^*). \end{aligned} \quad (2.7)$$

For given B we have to find $\phi_1^s, \phi_2, \psi_1^*, \psi_2^*$ and locations d_j of SBs on z axis. Choose a reference frame in such a way that $z(\phi_2) = 0$. According to (2.2-2.4), we have $z(\phi) = M(S_H \phi, B) - M(S_H \phi_2, B)$. Thus, solving another three equations,

$$Z_2(\psi_2^*) = -d_2, \quad r(\phi_2) = R_2(\psi_2^*), \quad \theta(\phi_2, \psi_2^*) = \theta_2, \quad (2.8)$$

we find ψ_2^*, ϕ_2 and d_2 as explicit (or implicit) expressions. Resolving now the two first equations in (2.7) w.r.t. ϕ_1^s and ψ_1^* we find them also as explicit (or implicit) expressions.

The shift d_1 follows from the third equation in (2.7), $d_1 = z(\phi_1^s, \phi_2) - Z_1(\psi_1^*)$. The computation of ϕ_1^s and ψ_1^* can be performed as follows. First, note that $rr' = B \sin(S_H \phi)$, and $rz' = 1 + B \cos(S_H \phi)$. From (2.4) we obtain $2B \cos(S_H \phi_1^s) = R^2(\psi_1^*) - 1 - B^2$, and find

$$2B \sin(S_H \phi_1^s) = \pm \sqrt{[R^2(\psi_1^*) - (1 - B)^2][(1 + B)^2 - R^2(\psi_1^*)]},$$

where the sign is determined by the value of ϕ_1^s . Thus, the first equation in (2.7) reads

$$\begin{aligned} \pm Z_1'(\psi_1^*) \sqrt{[R^2(\psi_1^*) - (1 - B)^2][(1 + B)^2 - R^2(\psi_1^*)]} = \\ R_1'(\psi_1^*) [R^2(\psi_1^*) + 1 - B^2], \end{aligned}$$

and it should be resolved w.r.t. ψ_1^* in the prescribed range of the values of ψ_1 . Substitution of this value ψ_1^* into condition $2B \cos(S_H \phi_1^s) = R^2(\psi_1^*) - 1 - B^2$, allows to compute ϕ_1^s . Similarly one can obtain the relation describing the condition $\theta_2 = 0$.

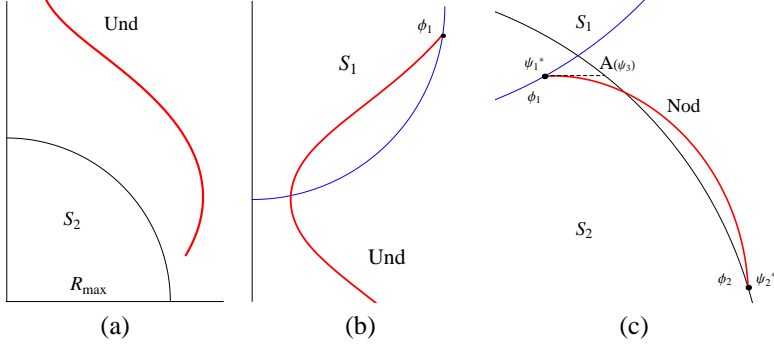


FIGURE 2. Sketches of menisci which have not physical meaning due to the different reasons: (a) meniscus does not reach the solid surface S_2 , (b) meniscus reaches solid surface S_1 with negative contact angle and (c) meniscus reaches S_1 at the endpoint which is immersed in S_2 .

After obtaining the value ϕ_j^s one has to check if the meniscus arrives at the corresponding SB is indeed outside of the SB. To do this introduce $z^* = z(\phi_j^s) + \delta z_j$, $\delta z_j = (-1)^j \delta z$, such that also $Z_j^* = Z_j(\psi_j^*) + \delta z_j$. Writing

$$z(\phi_j^s + \delta\phi_j) = z(\phi_j^s) + \delta z_j, \quad Z_j(\psi_j^* + \delta\psi_j) = Z_j(\psi_j^*) + \delta z_j,$$

express $\delta\psi_j \ll 1$ in the linear approximation $\delta\phi_j = \delta z_j / z'(\phi_j^s)$, $\delta\psi_j = \delta z_j / Z_j'(\psi_j^*)$. Write down the radial coordinates of the meniscus and the SB at $z = z^*$:

$$\begin{aligned} r(\phi_j^s + \delta\phi_j) &= r(\phi_j^s) + r'(\phi_j^s)\delta\phi_j + r''(\phi_j^s)\delta\phi_j^2/2, \\ R_j(\psi_j^* + \delta\psi_j) &= R_j(\psi_j^*) + R_j'(\psi_j^*)\delta\psi_j + R_j''(\psi_j^*)\delta\psi_j^2/2. \end{aligned} \quad (2.9)$$

Calculate a difference,

$$r(\phi_j^s + \delta\phi_j) - R_j(\psi_j^* + \delta\psi_j) = \left[\frac{r''(\phi_j^s)}{z'^2(\phi_j^s)} - \frac{R_j''(\psi_j^*)}{Z_j'^2(\psi_j^*)} \right] \frac{\delta z_j^2}{2}, \quad (2.10)$$

which sign is defined by the expression in the square brackets. As the meniscus is outside of the SB when this difference is positive we obtain substituting (2.4) into (2.10) the following condition

$$\delta\rho = \frac{r''(\phi_j^s)}{z'^2(\phi_j^s)} - \frac{R_j''(\psi_j^*)}{Z_j'^2(\psi_j^*)} = -\frac{r^2(\phi_j^s)B \cos \phi_j^s + B^2 \sin^2 \phi_j^s}{r(\phi_j^s)(1 + B \cos \phi_j^s)^2} - \frac{R_j''(\psi_j^*)}{Z_j'^2(\psi_j^*)} > 0, \quad (2.11)$$

or its equivalent

$$\delta\rho^* = \frac{r''(\phi_j^s)}{r'^2(\phi_j^s)} - \frac{R_j''(\psi_j^*)}{R_j'^2(\psi_j^*)} = -\frac{1}{r(\phi_j^s)} \left[1 + \frac{r^2(\phi_j^s)B \cos \phi_j^s}{B^2 \sin^2 \phi_j^s} \right] - \frac{R_j''(\psi_j^*)}{R_j'^2(\psi_j^*)} > 0. \quad (2.12)$$

The derived conditions (2.11,2.12) are particular cases of a more general case when the meniscus is partially immersed into SB.

• **Type C:** *meniscus reaches one SB at the endpoint which is immersed into the other SB, Figure 2c*

Let a lower of two intersecting SB be "pierced" by meniscus. Choose a reference frame in such a way that $z(\phi_2) = d_2 + Z_2(\psi_2^*) = 0$. A point $A(\psi_3) \in S_2$ is located at $\{R_2(\psi_3), d_2 + Z_2(\psi_3) = z(\phi_1)\}$ where $z(\phi_1) = M(S_H\phi_1, B) - M(S_H\phi_2, B)$. The meniscus does not exist if $R_2(\psi_3) > R_1(\psi_1^*) = r(\phi_1)$. Summarizing necessary formulas we arrive at requirements of meniscus nonexistence

$$\begin{aligned} Z_2(\psi_3) - Z_2(\psi_2^*) &= \Delta(\phi_1, \phi_2, S_H, B), \\ R_2(\psi_2^*) &= r(\phi_2), \quad R_2(\psi_3) > r(\phi_1). \end{aligned} \quad (2.13)$$

Using an invariance of nonexistence phenomenon under permutation the upper and lower SB write the requirements of meniscus nonexistence when an upper of two intersecting SB is "pierced" by meniscus,

$$\begin{aligned} Z_1(\psi_3) - Z_2(\psi_1^*) &= -\Delta(\phi_1, \phi_2, S_H, B), \\ R_1(\psi_1^*) &= r(\phi_1), \quad R_1(\psi_3) > r(\phi_2). \end{aligned} \quad (2.14)$$

• **Type D:** *the center of S_2 is above the center of S_1 , Figure 3a*

This leads to meniscus that reaches S_1 at the endpoint which is immersed in S_2 and reaches S_2 at the endpoint which is immersed in S_1 . To find the restricting relation make use of (2.3) and eliminate there ψ_j^* . Thus, we arrive at the restricting relation ($d_1 = d_2$),

$$\begin{aligned} z_1(\phi_1) - z_2(\phi_2) &= \Delta(\phi_1, \phi_2, S_H, B) = Z_1(\psi_1^*) - Z_2(\psi_2^*), \\ \psi_j^* &= R_j^{-1}[r_j(\phi_j)]. \end{aligned} \quad (2.15)$$

where f^{-1} denotes the inverse function w.r.t. f .

3. Existence of axisymmetric menisci between two spheres

In this section we specify formulas (2.6-2.14) for two solid spheres given by following formulas,

$$R_j(\psi_j) = a \sin \psi_j, \quad Z_j(\psi_j) = (-1)^j a \cos \psi_j. \quad (3.1)$$

3.1. Constraints of A and B types

There exists a critical angle ϕ_A related to the menisci nonexistence of type type **A** (see Figures 2a). It corresponds to a meniscus which does not reach a solid sphere with radius a ,

$$a^2 = 1 + B^2 + 2B \cos \phi_A \quad \rightarrow \quad \cos \phi_A = (a^2 - 1 - B^2)/2B. \quad (3.2)$$

A critical angle ϕ_B of the type **B** corresponds to the meniscus on Figure 2b. To calculate it use the relations

$$\frac{R'(\psi_B^*)}{Z'(\psi_B^*)} = \frac{r'(\phi_B^*)}{z'(\phi_B^*)}, \quad r(\phi_B) = R(\psi_B^*), \quad z(\phi_B) = d + Z(\psi_B^*), \quad (3.3)$$

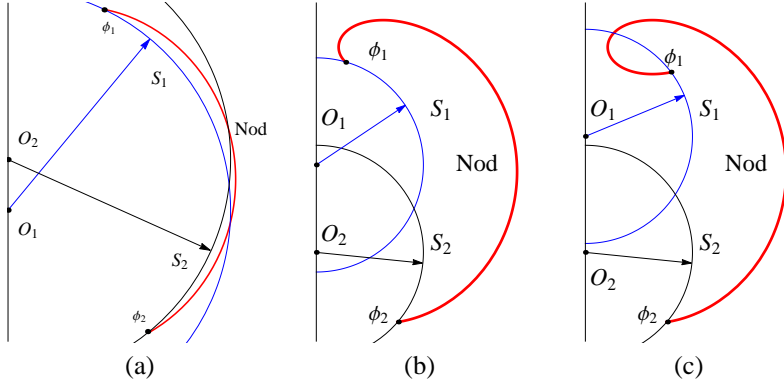


FIGURE 3. (a) Sketch of B-B meniscus forbidden due to the exchange of the SB centers. Sketch of two B-B menisci which (b) has and (c) has not physical meaning. In the latter case a meniscus pierces S_1 at its back at the endpoint ϕ_1 : $\pi < \phi_1 < 2\pi - \arccos \left[-(1 + a + B^2)/(B(2 + a)) \right]$.

in (2.4, 3.1) and obtain for menisci with positive curvature ($S_H = 1$),

$$\tan \psi_B^* = \mp \frac{1 + B \cos \phi_B}{B \sin \phi_B}, \quad \sin \psi_B^* = \frac{\sqrt{1 + B^2 + 2B \cos \phi_B}}{a}, \quad (3.4)$$

where + (-) sign corresponds the lower (upper) sphere. Eliminating of ψ_B^* from (3.4) we obtain

$$\cos \phi_B = -\frac{1 + B^2 + b}{B(2 + b)}, \quad b = \pm a. \quad (3.5)$$

When $2 + b > 0$, represent (3.5) as follows

$$B(2 + b) > 1 + B^2 + b > -B(2 + b) \quad \rightarrow \quad \begin{cases} (1 - B)(1 - B + b) < 0, \\ (1 + B)(1 + B + b) > 0. \end{cases}$$

In case of **Und** we have a negative $b = -a$,

$$B < 1, \quad -2 < b < B - 1, \quad -B - 1 < b \rightarrow \\ 1 - B < a < \min\{1 + B, 2\} = 1 + B. \quad (3.6)$$

In case of convex **NOD** we have a positive $b = a$,

$$B > 1, \quad b > B - 1 > -B - 1 \quad \rightarrow \quad a > B - 1. \quad (3.7)$$

When $2 + b < 0$, represent (3.5) as follows

$$-B(2 + b) > 1 + B^2 + b > B(2 + b) \quad \rightarrow \quad \begin{cases} (1 - B)(1 - B + b) > 0, \\ (1 + B)(1 + B + b) < 0. \end{cases}$$

In case of **Und** we have a negative $b = -a$,

$$B < 1, \quad B - 1 < b < -1 - B, \quad b < -2, \quad \rightarrow \\ \max\{1 + B, 2\} = 2 < a < 1 - B, \quad (3.8)$$

which is a contradiction. In case of convex Nod we have a negative $b = -a$,

$$\begin{aligned} B > 1, \quad b < -B - 1 < B - 1, \quad b < -2, \quad \rightarrow \\ a > \max\{B + 1, 2\} = B + 1. \end{aligned} \quad (3.9)$$

We have to make certain that all menisci have a physical meaning. Namely, we require that the menisci approaching contact point on the sphere with ϕ_B given by (3.5) are outside of the sphere. As $R_j''(\psi_j^*)/Z_j'^2(\psi_j^*) = -1/R_j(\psi_j^*) = -1/r(\phi_j^s)$, using the condition (2.11) we find

$$\begin{aligned} r(\phi_B)\delta\rho &= 1 - \frac{B \cos \phi_B(1 + B^2 + 2B \cos \phi_B) + B^2 \sin^2 \phi_B}{(1 + B \cos \phi_B)^2} \\ &= \frac{1 - B^2}{1 + B \cos \phi_B} = 2 \mp a, \end{aligned} \quad (3.10)$$

where the "+" sign is selected for Nod in (3.7), and the "-" sign stands for Und in (3.6) and Nod in (3.9). In the last case $a > 2$, so that the Nod meniscus in (3.9) approaches the contact point immersed into the sphere and thus it should be removed from further consideration.

Summarize (3.6, 3.7). The menisci exist when

$$\begin{aligned} \text{Und} : \left\{ \begin{array}{l} B < 1, \\ |a - 1| < B, \end{array} \right. & \left\{ \begin{array}{l} \cos \phi_B = -\frac{1+B^2-a}{B(2-a)}, \\ 1 + B \cos \phi_B = \frac{1-B^2}{2-a}, \end{array} \right. \\ \tan^2 \psi_B^* &= \frac{1 - B^2}{B^2 - (a - 1)^2}, \end{aligned} \quad (3.11)$$

$$\begin{aligned} \text{Nod} : \left\{ \begin{array}{l} B > 1, \\ a + 1 > B, \end{array} \right. & \left\{ \begin{array}{l} \cos \phi_B = -\frac{1+B^2+a}{B(2+a)}, \\ 1 + B \cos \phi_B = \frac{1-B^2}{2+a}, \end{array} \right. \\ \tan^2 \psi_B^* &= \frac{B^2 - 1}{(a + 1)^2 - B^2}. \end{aligned} \quad (3.12)$$

A choice of the sign of $\tan \psi_B^*$ is dictated by the value of ϕ_B running in the range $[0, 2\pi]$. To choose a correct sign introduce for *the upper and lower spheres* two variables σ_1 and σ_2 , respectively. The ranges $0 \leq \psi_B^* \leq \pi/2$ ($\sigma_j = 1$) and $\pi/2 \leq \psi_B^* \leq \pi$ ($\sigma_j = -1$) are called the *face* side and *back* side of sphere, respectively. Thus, σ_1 and σ_2 are valuated as follows,

$$\begin{aligned} \text{upper sphere, face side (F)} &\rightarrow \sigma_1 = 1, \\ \text{upper sphere, back side (B)} &\rightarrow \sigma_1 = -1, \\ \text{lower sphere, face side (F)} &\rightarrow \sigma_2 = 1, \\ \text{lower sphere, back side (B)} &\rightarrow \sigma_2 = -1. \end{aligned} \quad (3.13)$$

Bearing in mind that $1 + B^2 - a$ in (3.11, 3.12) may obtain both positive and negative values, the ranges of variation of ϕ_B may be specified if all restrictions on a, B

would be taken into account (see Table below).

PR	Und	Und	Nod, $H > 0$	Nod, $H < 0$
	$B^2 < a - 1 < B$	$-B < a - 1 < B^2$	$B < a + 1$	$B < a + 1$
F/B	$\sigma_2 = 1$ or $\sigma_1 = -1$			$\sigma_1 = 1$ or $\sigma_2 = -1$
ϕ_B	$[0, \pi/2] \pm 2\pi$	$[\pi/2, \pi] \pm 2\pi$	$[\pi, 3\pi/2] \pm 2\pi$	$[\pi/2, \pi] \pm 2\pi$
F/B	$\sigma_2 = -1$ or $\sigma_1 = 1$			$\sigma_2 = 1$ or $\sigma_1 = -1$
ϕ_B	$[3\pi/2, 2\pi] \pm 2\pi$	$[\pi, 3\pi/2] \pm 2\pi$	$[\pi/2, \pi] \pm 2\pi$	$[\pi, 3\pi/2] \pm 2\pi$

A concave Nod ($S_H = -1$) is considered separately. In (3.4, 3.5) the first formula in (3.4) is changed,

$$\tan \psi_B^* = \pm \frac{1 + B \cos \phi_B}{B \sin \phi_B}, \quad b = a, \quad (3.14)$$

where - (+) sign corresponds to the lower (upper) sphere. Keeping in mind that only the face sides of lower and upper spheres are permitted for concave NOD we arrive at the range of ϕ_B given in Table above, where a symbol $[\gamma_1, \gamma_2] \pm 2\pi$ denotes three different ranges: $[\gamma_1, \gamma_2]$, $[\gamma_1 + 2\pi, \gamma_2 + 2\pi]$ and $[\gamma_1 - 2\pi, \gamma_2 - 2\pi]$. See Figure 3c where $\phi_1 \in [\pi, 3\pi/2]$ and $\phi_2 \in [-\pi, -3\pi/2]$.

According to [2], section 6.2, there exist the Und and Nod menisci with completely concave meridional profiles (without IP, see Figure 1a) which are allowed for the F-F spheres arrangement. Such menisci do exist in the F-B arrangements if the spheres radii a_j and menisci parameter B satisfy,

$$\text{Nod} : \arccos \left(-\frac{1 + B^2 + a_1}{B(2 + a_1)} \right) < \arccos \left(-\frac{1 + B^2 + a_2}{B(2 + a_2)} \right), \quad (3.15)$$

$$a_1 > a_2,$$

$$\text{Und} : \arccos \left(-\frac{1 + B^2 - a_1}{B(2 - a_1)} \right) > \arccos \left(-\frac{1 + B^2 - a_2}{B(2 - a_2)} \right),$$

$$a_1 > a_2.$$

According to (3.15) both concave menisci (Und and Nod) do not exist in the F-B arrangement if $a_1 = a_2$. In Figure 4 we present two concave menisci in the F-B arrangement of spheres with zero contact angles. Finally, in case of the B-B spheres

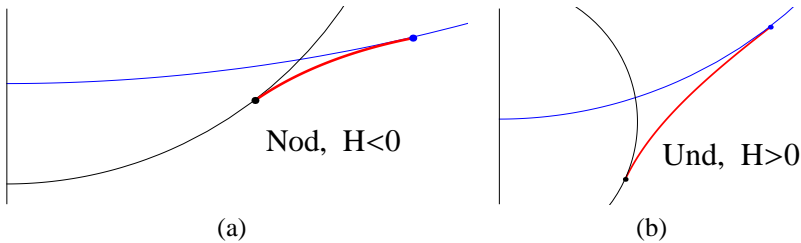


FIGURE 4. Two concave menisci in the F-B setup between two spheres: a) Nod, $B = 1.2$, $a_1 = 2.2$, $a_2 = 0.5$, $\phi_1^* = 204^\circ$, $\phi_2^* = 192^\circ$; b) Und, $B = 0.8$, $a_1 = 0.8$, $a_2 = 0.25$, $\phi_1^* = 209^\circ$, $\phi_2^* = 187^\circ$.

setup the existence of the concave menisci is forbidden.

3.2. Constraint of C type

The conditions (2.13,2.14) derived for the third case of meniscus nonexistence reduce to the following relations for $1 < B < a_i + 1$ in an assumption that the meniscus does not "pierce" the i -th SB:

$$M(S_H\phi_1, B) - M(S_H\phi_2, B) + [\sigma_I A_i(\phi_I) - A_i(\phi_i)] = 0, \quad (3.16)$$

$$A_i(\phi_j) = \sqrt{a_i^2 - (1 + B^2 + 2B \cos \phi_j)}, \quad I = (i + 1)(\text{mod} 2).$$

Coexistence of the **A**, **B** and **C** types of constraints may be found in Figure 10.

3.3. Constraint of D type

Substitute (2.4, 3.1) into (2.15) and obtain the condition of the proper SB positioning,

$$M(S_H\phi_1, B) - M(S_H\phi_2, B) + \sigma_1 A_2(\phi_1) + \sigma_2 A_1(\phi_2) = 0. \quad (3.17)$$

Coexistence of the **A**, **B** and **D** types of constraints may be found in Figures 13c and 14c,d. In Figure 5 we present two typical domains of menisci existence.

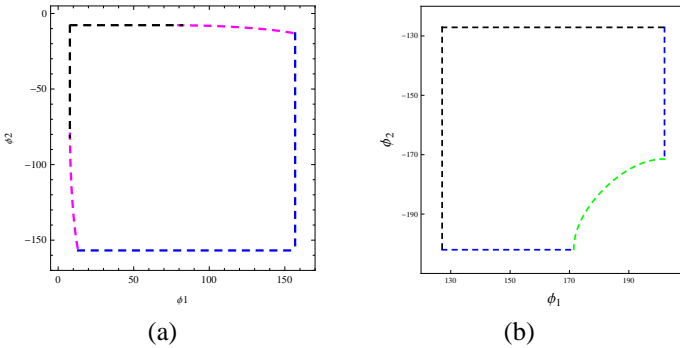


FIGURE 5. Coexistence of the **A** (black), **B** (blue), **C** (magenta) and **D** (green) types constraints for Nod between two equal spheres: (a) F-F setup, $B = 1.205, a = 2.2$; (b) B-B setup, $B = 1.5, a = 1.2$.

4. Menisci between equal spheres. Face-to-Face setup

In the following we present a gallery of images showing for given value of B in the plane $\{\phi_1, \phi_2\}$ the regions of existence (limited by the dashed curves) and inside them the regions of stability (shading shown in *blue* for $S_H = 1$ and in *light orange* for $S_H = -1$). These images should not be understood as solution of the problem of meniscus existence between the two solid spheres at a given distance d between their centers with prescribed contact angles θ_i . On the contrary, a point (ϕ_1, ϕ_2) in the region of existence determines an axisymmetric meniscus with a meridional

profile given by (2.4) for $\phi_2 \leq \phi \leq \phi_1$. This meniscus makes some contact angles θ_i with the solid spheres which can be computed using simple trigonometric relations, while the distance d is computed from (2.3). If this point appears in the shaded area the corresponding meniscus is stable.

The *red* curves in Figures show the location of Stab domain boundary for the menisci with the fixed CL with SB. The *brown* lines show the change in the number of IP in the meridional Und profile. The number of IPs in Und profile is denoted in *red*, e.g., 2^+ means two IPs on the meniscus meridional section M which is convex in vicinity of $\phi = \phi_1$ and 1^- means one IP on M which is concave in vicinity of $\phi = \phi_1$. Four different types of meniscus existence boundaries are denoted in *black* (**A**), *blue* (**B**), *magenta* (**C**) and *green* (**D**) colors. In the first series of the images in Figure 6, the coordinates ϕ_1, ϕ_2 are labeled, but further on they are dropped to improve a visual perception.

4.1. Unduloidal menisci between two solid spheres

In this section we present the stability diagrams for Und menisci between two equal spheres. These diagrams were found by analyzing a positiveness of the matrix Q_{ij} in (1.1). In Figure 6 and Figure 8 a,b such diagrams are presented for a wide range of B . In the case $B = a - 1$ we find another phenomenon: the boundaries of stability domains for fixed and free CL meet (this question was left open in [2]). In all cases there exist three kinds of stable Und menisci: without IPs and with one or two IPs.

Instability of Und menisci with more than one IP became a sort of folklore although there is no any rigorous claim in this regards. E.g., dealing with menisci between solid sphere contacting the plate the authors [6] posed a statement which was not supported by calculation: "There might be more than one IP . . . Multiple IPs in the meridional profiles are known but such menisci are likely to be unstable". Although in [2] we have shown that Und menisci with more than one IP between two solid parallel plates are always unstable, the general statement for two arbitrary SB remains elusive.

A strong statement about stability of axisymmetric menisci between two solid spheres has been announced in [12], namely, Theorem at p.374 in [12] and its equivalent version at p.397 in [13] reads: "the convex Und or Sph menisci are stable, while the convex Nod meniscus is unstable. The solid spheres have not to be equal or have equal contact angles". The examples of the stable convex and concave Und menisci with two IP are shown in Figure 7c,d.

4.2. Nodoidal menisci between solid spheres (2 types of constraints)

Considering the NOD menisci it should be underlined that part of the plane $\{\phi_1, \phi_2\}$ where the meniscus with $S_H = -1$ exists is determined by relation (2.5) and the existence conditions. The Stab domain (shown in *light orange*) covers either a part of (Figure 8c) or the whole Exst (Figure 8d). The same time the convex NOD menisci with $S_H = 1$ for $1 < a < 2$ appear to be stable everywhere they exist (Figure 8c,d). Examples of the stable NOD menisci are shown in Figure 9.

4.3. Nodoidal menisci between solid spheres (3 types of constraints)

For some parameter values one can observe a special case when Exst domain is bounded by three types of constraint. Such an example is illustrated in Figure 10

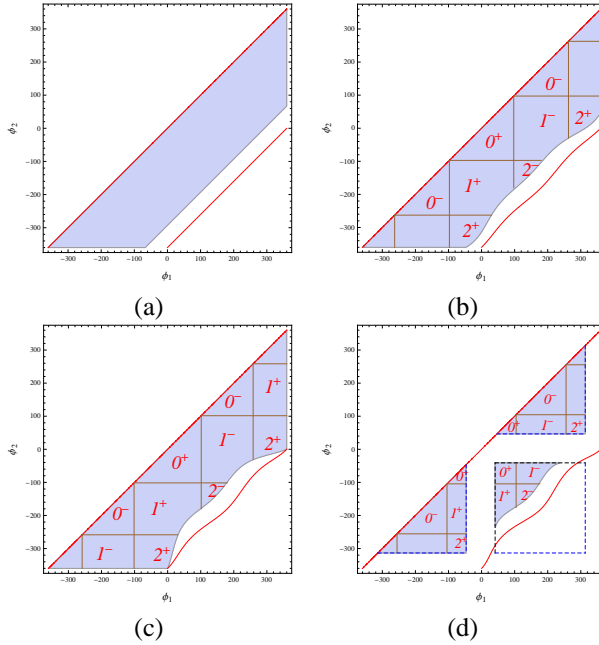


FIGURE 6. Stability diagrams for F-F setup of (a) Cyl meniscus, $B = 0$, and three Und menisci, (b) $B = 0.15$, (c) $B = 0.2$ and (d) $B = 0.25$, between two solid spheres of radius $a = 1.2$. The number of IPs in Und profile is denoted in red throughout the whole manuscript.

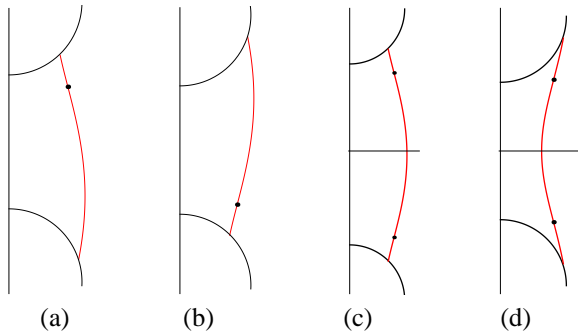


FIGURE 7. Stable Und menisci $B = 0.25$ with one and two IPs (black points) for F-F setup between two solid spheres of radius $a = 1.2$ and endpoints: (a) 1^- , $\phi_2 = -60^\circ$, $\phi_1 = 135^\circ$, (b) 1^+ , $\phi_2 = 60^\circ$, $\phi_1 = -135^\circ$, (c) 2^- , $\phi_2 = -135^\circ$, $\phi_1 = 135^\circ$ and (d) 2^+ , $\phi_2 = 60^\circ$, $\phi_1 = 300^\circ$.

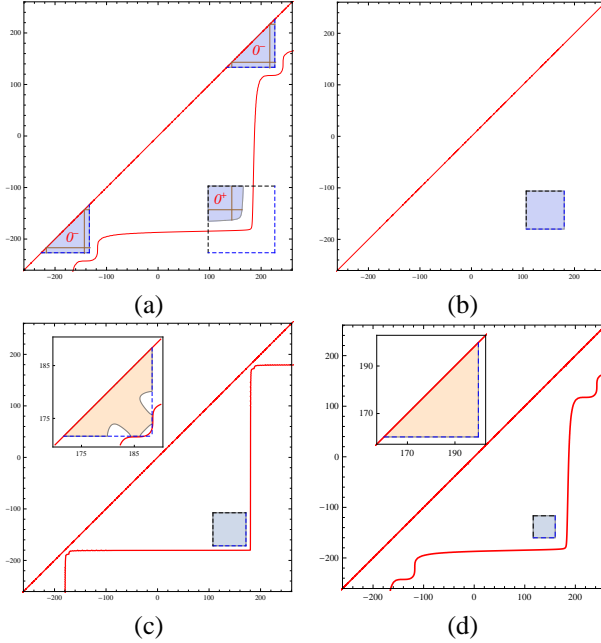


FIGURE 8. Stability diagrams for F-F setup of (a) **Und** meniscus, $B = 0.8$, (b) **Sph** meniscus, $B = 1$, and two **Nod** menisci, (c) $B = 1.03$, (d) $B = 1.25$, between two solid spheres of radius $a = 1.2$.

where **Exst** and **Stab** regions for the **NOD** menisci are shown. Note that the concave **Nod** meniscus for $B = 1.05$ is unstable in small part of **Exst**, while for larger values of B these menisci are stable everywhere in the corresponding **Exst** region.

4.4. Menisci between two equal contacting spheres

In this section we analyze a special case of liquid bridges between two equal contacting spheres to check recent claims made in [14]. For convenience we make use of menisci classification given independently in [7] and [13]. Following formulas (6,7) in [7] define α as a real root of equation,

$$1 + 4\alpha(\alpha - 1) \sin^2(\theta + \psi) = B^2, \quad \theta = \theta_1 = \theta_2, \quad \psi = \psi_1 = \psi_2. \quad (4.1)$$

	Nod ⁻	Cat	Und	Cyl	Und	Sph	Nod ⁺
α	< 0	0	$(0, 1/2)$	$1/2$	$(1/2, 1)$	1	> 1
B	> 1	—	$(0, 1)$	0	$(0, 1)$	1	> 1

This produces a correspondence $\alpha \leftrightarrow B$ (excluding the **Cat** meniscus). The only difference with [13] is that it used $A = -\alpha$, where **Cyl** occurs only if $\theta + \psi = \pi/2$ and **Nod**[±] denote the nodoid menisci with negative (-) or positive (+) curvature H , respectively. A sequence of menisci listed in Table is presented in Figure 6 in

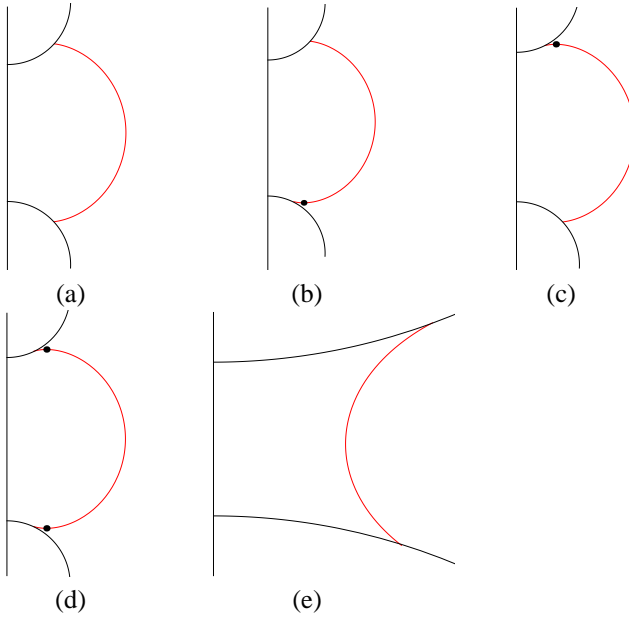


FIGURE 9. Stable convex NOD menisci $B = 1.25$ with one and two IPs and without IPs for F-F setup between two spheres of radius $a = 1.2$ and endpoints (a) 0^+ , $\phi_2 = -135^\circ$, $\phi_1 = 135^\circ$, (b) 1^+ , $\phi_2 = -155^\circ$, $\phi_1 = 135^\circ$, (c) 1^- , $\phi_2 = -135^\circ$, $\phi_1 = 155^\circ$, (d) 2^- , $\phi_2 = -157^\circ$, $\phi_1 = 157^\circ$. Stable concave NOD meniscus (e) $B = 1.25$ between two spheres of radius $a = 1.2$ and endpoints $\phi_2 = 163^\circ$, $\phi_1 = 193^\circ$.

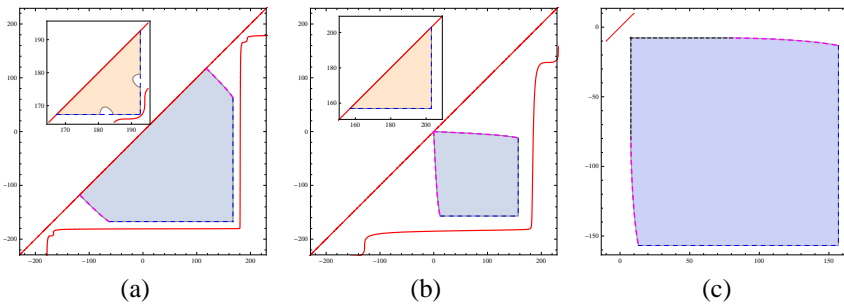


FIGURE 10. Stability diagrams for F-F setup of NOD menisci (a) $B = 1.05$, (b) $B = 1.2$, (c) $B = 1.205$ between two solid spheres of radius $a = 2.2$. In Figure 10c we focus on that part of stability domain which corresponds to the convex NOD: its boundaries comprise all three types of constraints.

[7]. The following statements about existence of axisymmetric menisci between two equal contacting spheres have been announced in [14]:

Theorem 3.3, 3.4. ‘For $\pi/2 < \theta < \pi$ and $\alpha < 0$ [Nod⁻] and $\pi/2 \leq \theta < \pi$ and $\alpha < 1$ [Nod⁻, Cat, Und, Cyl], no liquid bridge between contacting balls exists which is both axisymmetric and symmetric across the plane which is the perpendicular bisector of the line segment between the centers of the balls’.

Note 3.5. ‘For $\alpha > 1$ [Nod⁺], there may be axisymmetric bridges between contacting balls, but these are known to be unstable [12]. There do not exist stable axisymmetric bridges between contacting balls with: a) $\theta \geq \pi/2$, b) rotation symmetry, c) symmetry across the perpendicular bisector of the line segment between the centers of the balls. Open question: whether the last condition may be dropped’.

Consider the case when the meniscus has a contact angle with the sphere equal to $\pi/2$ and two spheres contact each other. The inclination angle α with the plane of the meniscus tangent at the contact point can be expressed through the similar angle ψ of the tangent to the sphere as follows: $\psi = \alpha \pm \pi/2$, where the lower (upper) sign is chosen for $0 \leq \psi \leq \pi/2$ ($\pi/2 \leq \psi \leq \pi$). The same time we have

$$\begin{aligned} -\frac{1 + B \cos \phi}{B \sin \phi} &= \tan \alpha, & a \sin \psi &= \sqrt{1 + B^2 + 2B \cos \phi}, \\ a - a \cos \psi &= M(\phi, B), \end{aligned} \quad (4.2)$$

where the last two equations determine the conditions $r(\phi) = R(\psi)$, $z(\phi) = Z(\psi)$ at the contact point. These equations produce

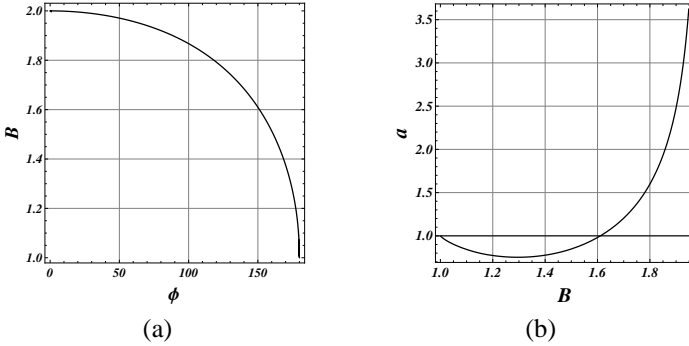


FIGURE 11. Plots $B = B(\phi)$ and $a = a(B)$ for contacting spheres and contact angles $\theta = 90^\circ$.

$$a = \frac{r^2(\phi) + M^2(\phi, B)}{2M(\phi, B)}, \quad \tan \psi = \frac{2r(\phi)M(\phi, B)}{r^2(\phi) - M^2(\phi, B)}. \quad (4.3)$$

Using the relation $\tan \psi = -\cot \alpha$ from the first equation in (4.2) we find

$$2(1 + B \cos \phi)r(\phi)M(\phi, B) = (r^2(\phi) - M^2(\phi, B)) B \sin \phi, \quad (4.4)$$

which allows to find for given B the coordinate ϕ of the contact point, and the sphere radius a . In Figure 11 we present the plots of implicit solutions of (4.3, 4.4). They both define a unique triple ϕ, B, a , for which such meniscus exists.

Another interesting case of contacting equal spheres of the radius a and the meniscus for $\phi_2 \leq \phi \leq \phi_1$ poses a question about a relation between ϕ_1 and ϕ_2 . The contact points on the spheres has the coordinates satisfying the relations:

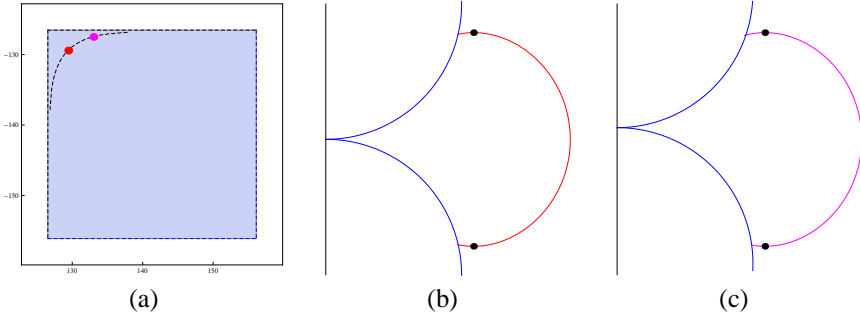


FIGURE 12. A stable domain (a) for Nod menisci ($B = 2.15$) with F-F setup between two touching spheres of radius $a = 1.75$ with (b) and without (c) symmetry across the perpendicular bisector of the line segment between the centers of the balls: (b) $\phi_1 = -\phi_2 \simeq 129.15^\circ$, $\psi \simeq 76^\circ$ and $\theta \simeq 115^\circ$; (c) $\phi_1 \simeq 133^\circ$, $\phi_2 \simeq -127.5^\circ$. *Red and magenta points* in (a) stand for stable menisci in (b) and (c), respectively.

$$r_i = a \sin \psi_i = \sqrt{1 + B^2 + 2B \cos \phi_i},$$

$$z_1 = M(\phi_1) = d_1 - a \cos \psi_1, \quad z_2 = M(\phi_2) = d_2 + a \cos \psi_2,$$

where d_i denotes the position of the i -th sphere center on the vertical axes, so that for the contacting spheres we have $d_1 - a = d_2 + a$, or $d_1 - d_2 = 2a$. The last equality leads to the desired relation

$$M(\phi_1) - M(\phi_2) = 2a - \sqrt{a^2 - (1 + B^2 + 2B \cos \phi_1)} - \sqrt{a^2 - (1 + B^2 + 2B \cos \phi_2)}. \quad (4.5)$$

In Figure 12 we present the stability diagram for Nod meniscus and label by *red and magenta* points (belonging to the *gray* curve defined by (4.5)) the location of stable menisci between two equal contacting spheres with contact angle $\theta > \pi/2$. This refutes the statement Note 3.5 in [14] in both cases: (b) with and (c) without symmetry across the perpendicular bisector of the line segment between the centers of the balls.

5. Menisci between equal spheres. Back-to-Back setup

A special version of the **B** type constraint in case of the NOD meniscus at the B-B spheres is presented in Figure 3. The stability analysis in this case is performed similarly to the case of F-F setup, but the sequence and structure of Stab with increasing value of B appears to be much simpler. One of the reasons of such simplification is

that the NOD meniscus with negative curvature is forbidden in this setup. To illustrate this point we consider three characteristic ranges of values of the solid sphere radius: $a < 1$, $1 < a < 2$, and $a > 2$. First consider the case $1 < a < 2$, choosing $a = 1.2$; the computation shows that the Und meniscus has no IPs and is stable everywhere it exists (Figure 13a). The NOD meniscus is stable in smaller part of the existence region Exst which boundary may be determined by the existence condition **D** (see Figures 13b,c).

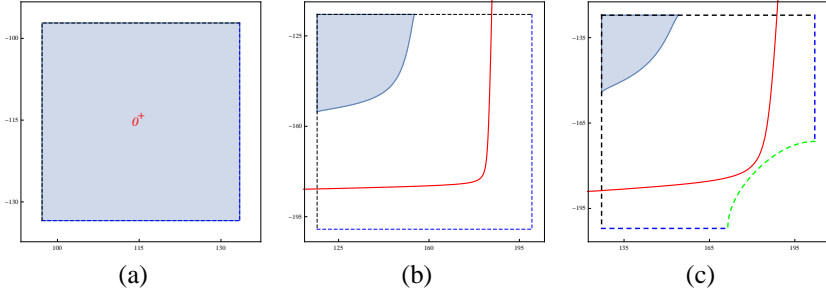


FIGURE 13. Stability diagrams for B-B setup of (a) Und meniscus, $B = 0.8$, and two NOD menisci, (b) $B = 1.25$, (c) $B = 1.5$, between two solid spheres of radius $a = 1.2$.

In the case $a < 1$ we observe that the Und meniscus has two IPs and again is stable everywhere it exists (Figure 14a); the same time Stab region of the convex NOD meniscus covers only some part of Exst (Figure 14b). Finally, when $a > 2$ the existence region of the NOD meniscus is strongly limited by the existence condition **D** and these menisci are stable in the large part of Exst (see Figure 14c,d).

6. Menisci between equal spheres. Face-to-Back setup

The F-B setup is quite simple for the analysis, as in this case the boundaries of Exst can be described as a "outer product" of the corresponding regions for F-F and B-B setups. To explain this feature consider the case when the meniscus touches the face of the upper SB at $\phi = \phi_1$, and the back of of the lower SB at $\phi = \phi_2$. The existence conditions **A** and **B** (represented by the black and blue broken lines) are determined for ϕ_1 and ϕ_2 independently. It is illustrated in Figure 15a and Figure 15b where the range of the accessible values for ϕ_1 is much larger than for ϕ_2 .

7. Menisci between nonequal spheres

The existence and stability analysis in the case of solid spheres of unequal radii is similar to the case of F-B setup considered in section 6. The boundaries of Exst determined by the conditions **A** and **B** depend on the corresponding sphere radii and have to be computed independently. This breaks the symmetry of Exst and Stab w.r.t. the line $\phi_1 + \phi_2 = 0$. A difference in spheres radii may lead to existence of special types of menisci which are forbidden in setup with equal radii.

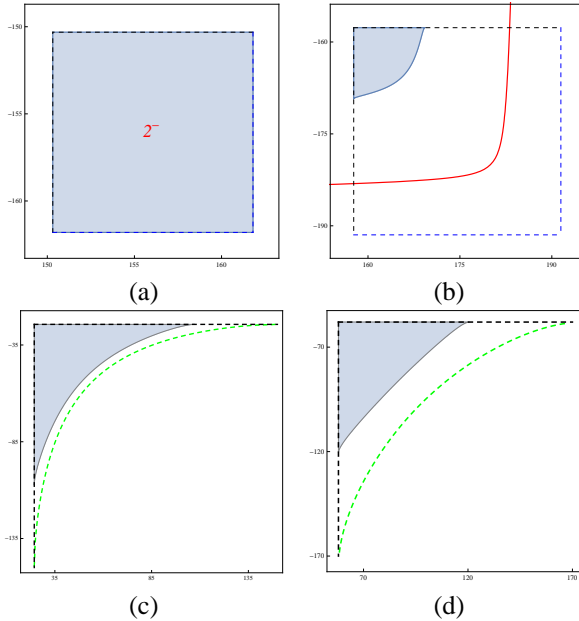


FIGURE 14. Stability diagrams for B-B setup of (a) Und meniscus, $B = 0.8$, and (b) Nod menisci, $B = 1.25$, between two solid spheres of radius $a = 0.5$. Stability diagrams for B-B setup of two Nod menisci, (c) $B = 1.25$, and (d) $B = 1.5$, between two solid spheres of radius $a = 2.2$.

7.1. Face-to-Face setup

In Figure 16 we present the stability diagrams for Und and Nod menisci for $1 < a_1 < 2$ and $a_2 > 2$. By comparison to Figures 6d and 16a; 8a and 16b; 10c and 16c, one may see how the stability diagrams become asymmetric w.r.t. to the line $\phi_1 + \phi_2 = 0$.

7.2. Face-to-Back setup

The F-B setup of menisci between two nonequal spheres gives rise to existence of concave NOD meniscus which is forbidden in F-B setup between two equal spheres (see Figure 16).

The trapezoidal geometry of Exst in Figure 17a appears due to intersection of triangular existence region for concave NOD meniscus in the F-F setup between two equal spheres of radius a_1 with existence constraint **A** on sphere of radius $a_2 < a_1$ that results in the triangle cut. Note that for the parameters selected in Figure 17a the concave NOD meniscus is stable in every point of Exst. In case of the convex NOD meniscus a part of the boundaries of Exst may be related to the **C** type constraint (see Figure 17c).

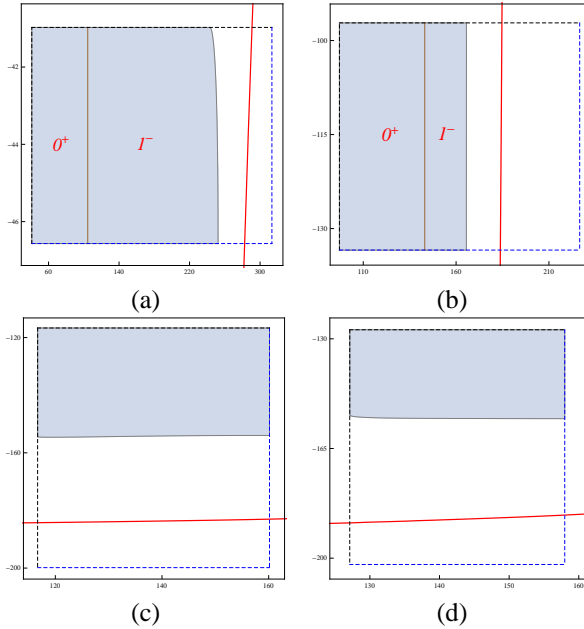


FIGURE 15. Stability diagrams for F-B setup of **Und** menisci, (a) $B = 0.25$ and (b) $B = 0.8$, and **Nod** menisci, (c) $B = 1.25$ and (d) $B = 1.5$, between two solid spheres of radius $a = 1.2$.

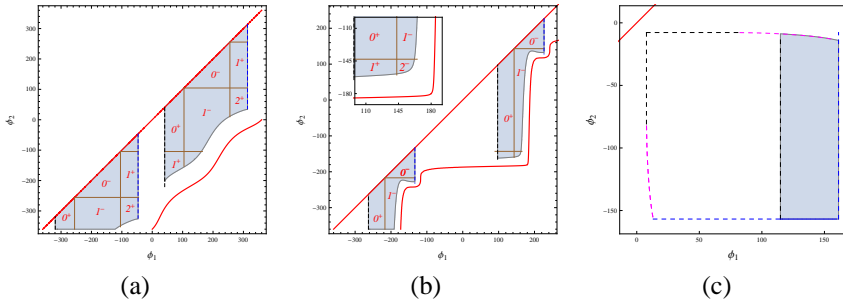


FIGURE 16. Stability diagrams for F-F setup of **Und** menisci, (a) $B = 0.25$, (b) $B = 0.8$, and **Nod** meniscus, (c) $B = 1.205$, between two nonequal solid spheres of radii $a_1 = 1.2$ and $a_2 = 2.2$.

Acknowledgement

The research was supported in part (LGF) by the Kamea Fellowship.

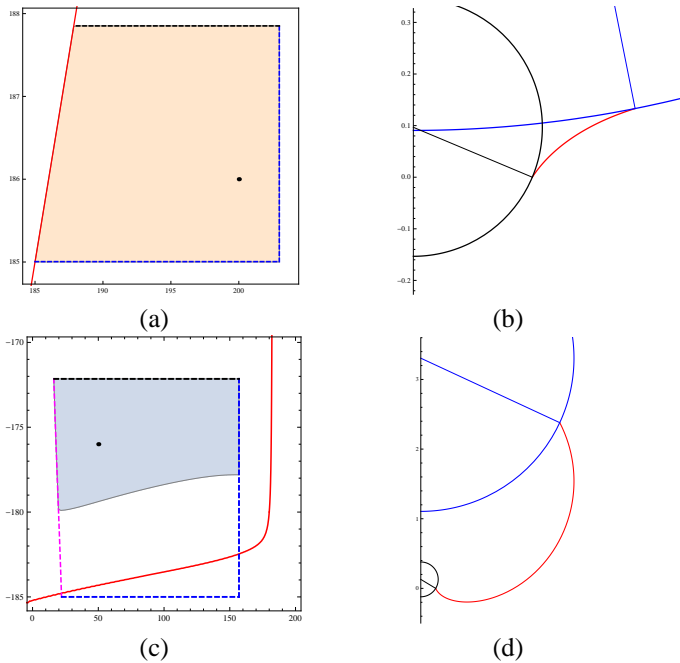


FIGURE 17. Stability diagrams for F-B setup of concave (a) and convex (c) Nod menisci, $B = 1.2$, between two non equal solid spheres of radii $a_1 = 2.2$ and $a_2 = 0.25$. Two stable Nod menisci, (b) $\phi_2 = 186^\circ$, $\phi_1 = 200^\circ$, and (d) $\phi_2 = -176^\circ$, $\phi_1 = 50^\circ$, are labeled by *black points* in diagrams. A *red line* in (a) is a main diagonal in the plane $\{\phi_1, \phi_2\}$. A *magenta curve* in (c) describes the *C* constraint of existence.

References

- [1] C.E. DELAUNAY, *Sur la surface de révolution dont la courbure moyenne est constante*, J. Math. Pure et App., **16** (1841), pp. 309-315.
- [2] L. FEL AND B. RUBINSTEIN, *Stability of Axisymmetric Liquid Bridges*, appear in Z. Angew. Math. Phys., <http://link.springer.com/article/10.1007/s00033-015-0555-5>
- [3] R. FINN AND T. VOGEL, *On the volume infimum for liquid bridges*, Z. Anal. Anwend., **11** (1992), pp. 3-23.
- [4] K. KENMOTSU, *Surfaces of revolution with prescribed mean curvature*, Tohoku Math. J., **32** (1980), pp. 147-153.
- [5] MYSHKIS, A.D., BABSKII, V.G., KOPACHEVSKII, N.D., L.A. SLOBOZHANIN, L.A. & TYUPTSOV, A.D.: *Lowgravity Fluid Mechanics*, Springer, New York (1987)
- [6] F. M. ORR, L. E. SCRIVEN AND A. P. RIVAS, *Pendular rings between solids: meniscus properties and capillary forces*, J. Fluid Mech., **67** (1975), pp. 723-744.
- [7] B. RUBINSTEIN AND L. FEL, *Theory of Axisymmetric Pendular Rings*, J. Colloid Interf. Sci., **417** (2014), pp. 37-50.

- [8] D. STRUBE, *Stability of spherical and catenoidal liquid bridge between two parallel plates in absence of gravity*, Micrograv. Sci. Technol., **4** (1991), pp. 263-269.
- [9] T. VOGEL, *Stability of a liquid drop trapped between two parallel planes*, SIAM J. Appl. Math., **47** (1987), pp. 516-525.
- [10] T. VOGEL, *Stability of a liquid drop trapped between two parallel planes, II: General contact angles*, SIAM J. Appl. Math., **49** (1989), pp. 1009-1028.
- [11] T. VOGEL, *Non-linear stability of a certain capillary problem*, Dynamics of Continuous, Discrete and Impulsive Systems, **5** (1999), pp. 1-16.
- [12] T. VOGEL, *Convex, Rotationally Symmetric Liquid Bridges between Spheres*, Pacific J. Math., **224** (2006), pp. 367-377.
- [13] T. VOGEL, *Liquid Bridges Between Balls: The Small Volume Instability*, J. Math. Fluid Mech., **15** (2013), pp. 397-413.
- [14] T. VOGEL, *Liquid Bridges between Contacting Balls*, J. Math. Fluid Mech., **16** (2014), pp. 737-744.
- [15] H. WENTE, *The symmetry of sessile and pendent drops*, Pacific J. Math., **88** (1980), pp. 387-397.
- [16] L. ZHOU, *On stability of a catenoidal liquid bridge*, Pacific J. Math. **178** (1997), pp. 185-198.

Boris Y. Rubinstein
Stowers Institute for Medical Research,
1000 E 50th St, Kansas City,
MO 64110, USA
e-mail: bru@stowers.org

Leonid G. Fel
Department of Civil Engineering,
Technion – Israel Institute of Technology,
Haifa, 32000, Israel
e-mail: lfel@technion.ac.il